Substituent Effects and the Energetics of Noncatalyzed Aryl Halide Aminations: A Theoretical Investigation

Supreeth Prasad, Dylan D. Rodene, Michael B. Burkholder, Kelling J. Donald,* and B. Frank Gupton*

Read Online

ACCESS | Metrics & More | Article Recommendations | Supporting Information

ABSTRACT: We report the influence of substituents and physical conditions on activation energies for the noncatalyzed amination (C−N cross-coupling reactions) of aryl halides. We uncover a significant correlation between the barrier heights of the C−N bond formation and Hammett σ parameters—a formal measure of the electron-withdrawing or -donating ability of substituents on the aryl halides. Our results indicate that such correlations are useful predictive tools for the amination of aryl halides over a wide range of substituent types. From 54 cases studied (six substituents occupying specific positions relative to halogen atoms), the 2-COOHPhI + $NH_2{}^nPr$ amination reaction is predicted to possess the lowest noncatalyzed activation free energy (135.6 kJ mol^{-1}) using the B3LYP method. The lower barriers for the 2-COOHPhX (for X = Cl, Br, and I) compounds are shown to originate from collusion between steric and electronic effects—specifically, the momentary formation of a hydrogen bond between an oxygen site on the *ortho*-COOH and the lone pair of the entering amine. Internal reaction coordinate (IRC) path calculations afforded us these and other key insights into the nature of the reactions. The control exerted by substituents on the arrangement of the transition state structure, as well as the sensitivity of the reaction barriers to temperature and solvent polarity, are discussed. These results offer new perspectives from which to assess the nature of the C−N bond formation and suggest new avenues for future exploration, especially in progress toward the metal-free amination of aryl compounds.
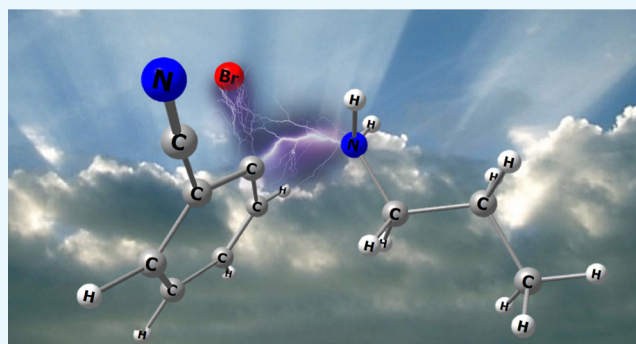
INTRODUCTION

The amination of aryl halides is of great importance to the discovery, development, and production of pharmaceuticals, as well as for the synthesis of a variety of other commodity chemicals with an *N*-aryl moiety.[1−3] A number of reaction schemes and methods for C−N bond formation of electron-rich aryl compounds—typically less reactive compounds under mild conditions than electron-poor aryl halides—have been developed.[4,5] Noteworthy amination reactions include the commonly implemented Ullmann and Goldberg reactions enabled by a copper-based reagent and a palladium-based Buchwald−Hartwig (BH) catalyst, respectively.[6,7]

The catalytic BH cross-coupling approach has been vital in unlocking limited and difficult synthetic transformations.[8−12] This approach has permitted the use of more diverse reagents and milder reaction conditions at an industrial scale.[13−16] Regardless of the broader substrate scope and functional group tolerance enabled by catalysts, alternative methodologies are being studied for the synthesis of *N*-aryl compounds, leading to greener chemistries.[17,18] In practice, transition metal-based amination reactions often require additional unit operations, such as the removal of any metal impurities and byproducts generated from the use of metal catalysts.

Compared to the BH approach, metal-free C−N coupling reactions have been sparingly reported in the literature.[19,20] More prevalent reports of metal-free aminations include microwave irradiation motifs[4,21−27] or base-catalyzed reaction schemes.[28−30] For example, microwave irradiation has been shown to enable direct metal-free coupling of morpholine to an aromatic ring containing free −OH and −NH_2 substituents (*i.e.*, strong electron-donating groups).[4] In addition, microwaves have been utilized to react aryl halide compounds containing a wide range of substituents. These reactants were able to produce good yields (≥61%) within short reaction times (≤20 min), except for the case of an acetyl substituted aryl compound.[4] This result, among others, indicates that microwave-assisted C−N aminations are capable of producing significant product yields under feasible reaction times while

simultaneously alleviating the need for excess product isolation steps when ran metal-free.

Theoretical methods provide us with an opportunity to quantify the kinetics and thermodynamics for model reaction systems, which aid in expanding upon conventional and alternative synthesis approaches, including those toward green chemistry. Previous C−N cross-coupling investigations have focused on studying the mechanism of aryl amination reactions, both experimentally[31−35] and computationally.[8,9,36−40] Yet, systematic computational investigations into the thermodynamics of the direct C−N bond formation remain sparse in the literature.

Herein, a theoretical investigation into the noncatalyzed amination of various substituted aryl halides as model compounds is presented. A diverse set of substituted aryl halides (RPhX for X = −Cl, −Br, and −I) was chosen to obtain a fundamental understanding of the influence of substituents on energy barriers and the kinetics of metal-free amination reactions between aryl halides and primary amines. The nature of the associated transition states for the substituents is evaluated. The Hammett σ constants for each substituent are ranked and compared with the respective activation energy barrier heights for the given reactions. Substituent placement (*ortho*-, *meta*-, and *para*-positions) was also accounted for to study the possible electronic and steric influences on the energy barrier heights. A brief assessment of the influence of temperature and solvent selection for the amination reactions is given. These results provide insights into a classic chemical reaction while raising considerations of utilizing substituents to influence chemical reactions. This work also provides a reference for future computational studies.

■ RESULTS AND DISCUSSION

The thermodynamics of the C−N bond formation between substituted benzene and amine derivatives were examined for the generalized reaction in Scheme 1 (*n*-RPhX + NH$_2$R′),

Scheme 1. Generalized Scheme of the Reaction between Substituted Aryl Halides and Various Primary Amines Considered in This Work
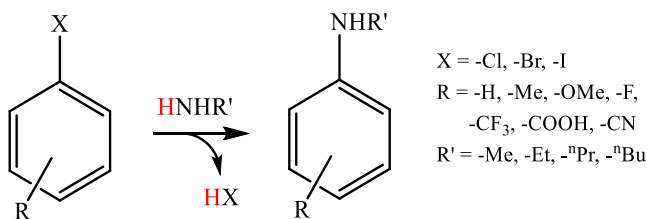
where n = 2 (*ortho*), 3 (*meta*) or 4 (*para*) for R = −H, −Me, −OMe, −F, −CF$_3$, −COOH, or −CN with X = −Cl, −Br, and −I. Fluorine (X = −F) was not included in this study as it is considered to be a poor leaving group for coupling reactions.[41,42]

The aryl substituents, R, were chosen for their relevance in the synthesis of active pharmaceutical ingredients as well as their ability to modulate the reactivity of the aryl ring.[43] Additionally, we consider a broad range of temperatures (−20, 25, and 80 °C) and solvation effects (relative permittivity—dielectric constants, ε_r = 1−78.36).

What Transition States Can Teach Us. To assess the mechanism and nature of the reaction shown in Scheme 1, IRC path calculations were carried out for all of the defined

substituted aryl halides. The IRC calculations were initiated using confirmed transition state structures (TSSs) to link the *n*-RPhX + NH$_2$R′ reactants with the *n*-RPhNHR′ + HX products.[44] Examples of the TSSs obtained are depicted in Figure 1. The TSSs from the QSTn calculations are consistent with nucleophilic aromatic substitution.[6] This pathway provided for a systematic approach to assess chemical reactivity and substituent effects of the aryl halide amination reactions. The full set of optimized cartesian coordinates for all of the reactants, products, and transition state structures are provided in Tables S10−S12 of the Supporting Information.

Each of the TSSs, as illustrated for the nine cases shown in Figure 1, shows the N atom of the amine coordinating to the C center bonded to the halogen atom of the aryl halide, with N···C separations equal to 1.90 ± 0.7 Å. During this process, the C center of the aryl halide undergoes a certain degree of rehybridization, such that the C−X bond rotates out of the plane of the ring to facilitate the initiation between the C center and the amine. In the mode of an addition−elimination reaction, the lone pair on the N is then donated to the C center, activating the C−X bond (*cf.* Figure 1), which ultimately leads to the migration of X from the aryl halide and a proton from the amine.

The extent of the C−X bond elongation in the optimized TSSs may be intuitively assumed to vary indirectly with the extent of the N → C "acid−base" interaction in preparation for X migration and C−N bond formation; however, this may not be the case. The C···X and N···C separations of the calculated TSSs, shown in Figure 1, were found to vary directly with each other for the combined n = 3 and 4 substituents, forming a remarkably linear relationship for each X (Figure 2d−f). Furthermore, the *meta*- and *para*-cases (i.e., n = 3, and 4) were linked by linear trends with surprisingly high coefficients of determination (R^2 = 0.992 to 0.970 for X = Cl to I). A direct and roughly linear trend was also observed for all ortho-cases (Figure 2a−c), with the exception of R = 2-COOH—an oddity that will be discussed further in later sections.

From Figure 2, it is clear that the identity of the R group only determines where the TSS geometry falls along the line of best fit. This suggests that all of the R groups inductively modify the electronic environment at the reaction site almost entirely via direct through-bond interactions (donating or withdrawing electron density) with no substantial secondary steric or other through-space effects that would be unique to individual R fragments. However, for the *ortho*-systems, the close proximity of the C−R and C−X bonds is such that steric effects and other weak interactions could have a particularly dramatic influence on the nature of the transition state structures, and those influences appear to be quite consequential for R = 2-COOH.

Beyond steric effects, the computational results provide structural evidence of a hydrogen bond between the saturated O center of the 2−COOH and one of the H−N bonds on the entering amine, as will be discussed in a later section. This interaction, we infer, accounts for the anomalous behavior of the 2-COOH TSS relative to the other ortho-cases shown in Figure 2. The overall effects of a hydrogen bond, electronic, and steric constraints sum to give a rather long C···N separation in the TSS of that 2-COOH system, much longer than expected, given the trend provided by the other data points shown in Figure 2 for the ortho-species. An alternative interpretation to consider is that the presence of an *ortho*-carboxyl group causes the C···X contact in the TSSs to be
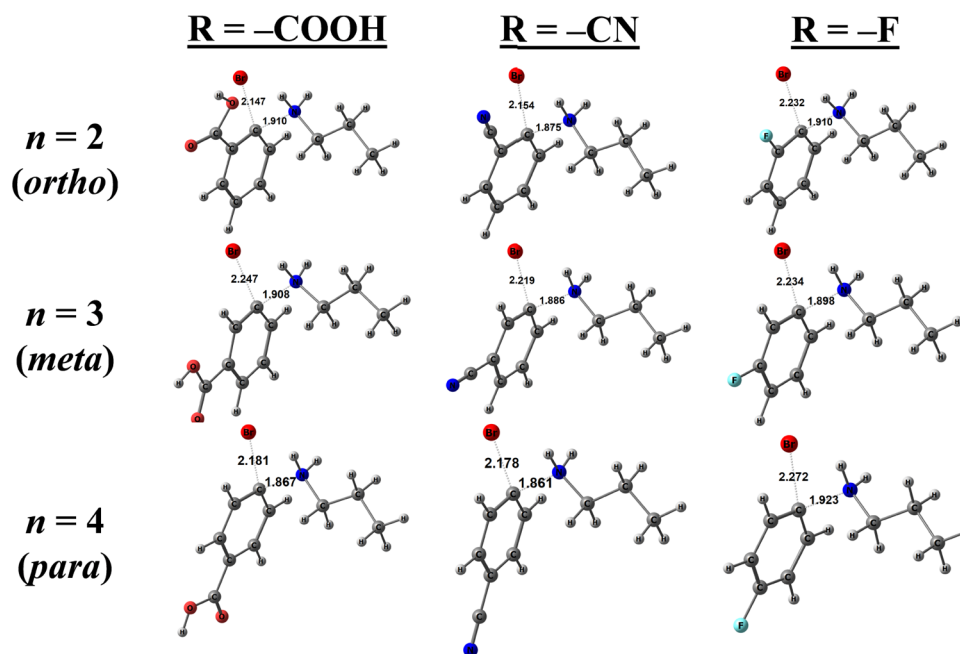
Figure 1. Transition state structures (TSSs) linking the reactants and products on the potential energy surfaces for the amination reactions, where *n* = 2 (*ortho*), 3 (*meta*), and 4 (*para*); R = −COOH, −CN, and −F; X = Br; and R′= ⁿPr. The cases shown here are qualitatively identical to all other systems investigated. Distances are presented in Å units.
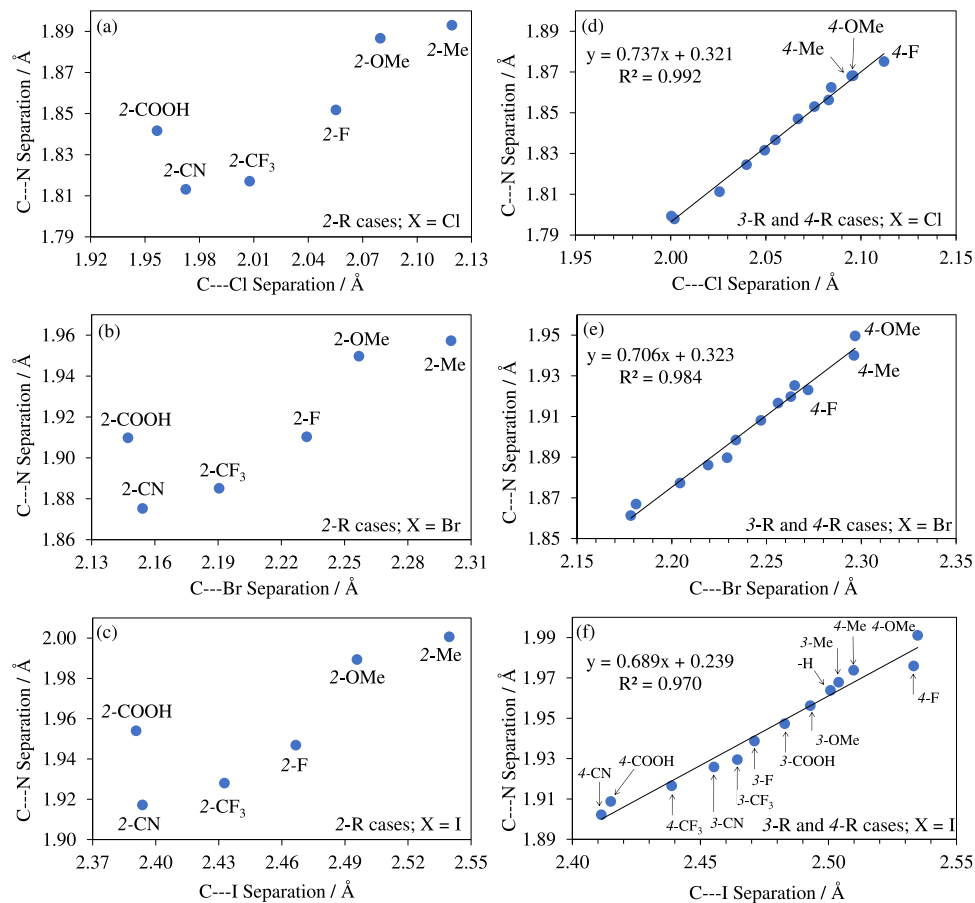
Figure 2. Correlations between the C⋯N and C⋯X separations in the transition state structures for the amination reactions for (a−c) *ortho*-cases and (d−f) *meta*-, *para*-, and unsubstituted (R = H) cases. The order of data points for the R groups is identical for all three plots (d−f), except for the last three data points of 4-F, 4-Me, and 4-OMe. To minimize congestion on the graphs (d−f) for *n* = 3, and 4, data points are explicitly labeled only for (f) X = I.

unduly short (relative to the C···N contact), but it is unclear from the transition structure what would account for a particular stubborn resistance to C···I bond breaking in the specific case of R = 2-COOH.

Curiously, the *ortho*- and *para*-TSSs (*i.e.*, the 2-R and 4-R systems) shown in Figure 2 span a somewhat larger range of C···X distances relative to the meta-cases (3-R). In Figure 2d–f, the *meta*-TSSs are nestled between the electron-donating 4-Me, 4-OMe, and 4-F groups (with the longest TSS contacts) and the electron-withdrawing groups (with the shortest contacts). These results show a link between the substituent position and TSS contacts, which presage a general relationship between the nature of the substitution pattern and the energetics of the amination reactions presented in the subsequent sections.

Quantifying the Barrier to Amination. Table 1 lists the activation energies (barrier heights) with zero-point energy

Table 1. Barrier Heights (E_a^{ZPE} and $\Delta G_a^{298.15\,K}$) for the Amination Reactions (n-RPhX + NH$_2$R′ → n-RPhNHR′ + HX), Where n = 2 (*ortho*), 3 (*meta*), and 4 (*para*); R = −CF$_3$, −CN, −COOH, −F, −Me, −OMe, and −H; X = −Cl, −Br, and −I; and R′ = −^{n}Pr

n-R	E_a^{ZPE} (kJ mol^{-1})			$\Delta G_a^{298.15\,K}$ (kJ mol^{-1})		
	X = Cl	X = Br	X = I	X = Cl	X = Br	X = I
2-CN	133.90	126.50	123.51	182.91	176.44	172.12
3-CN	151.29	141.45	137.77	200.49	189.85	186.19
4-CN	141.36	132.80	129.45	190.31	182.46	178.60
2-CF$_3$	139.62	129.82	125.95	190.05	179.86	176.50
3-CF$_3$	154.10	143.75	139.72	196.97	192.70	189.00
4-CF$_3$	148.14	138.01	135.07	198.46	182.54	183.42
2-COOH	120.61	112.19	108.99	173.84	163.78	159.76
3-COOH	158.33	147.49	143.12	206.94	195.18	191.24
4-COOH	142.83	133.62	130.57	192.98	181.89	180.25
2-F	156.22	146.09	142.04	204.38	194.42	189.55
3-F	156.43	145.96	141.45	205.13	194.79	189.51
4-F	173.71	156.09	155.92	223.30	203.88	204.90
-H	162.09	151.19	145.10	209.08	199.86	189.84
2-Me	166.17	152.86	145.07	215.25	201.57	192.69
3-Me	163.19	151.46	146.30	212.94	199.21	190.19
4-Me	166.90	160.08	149.41	216.15	209.82	198.81
2-OMe	163.90	152.17	147.07	212.03	199.62	195.22
3-OMe	161.86	150.62	145.27	210.42	198.43	193.15
4-OMe	180.39	162.35	156.49	225.69	209.43	204.13
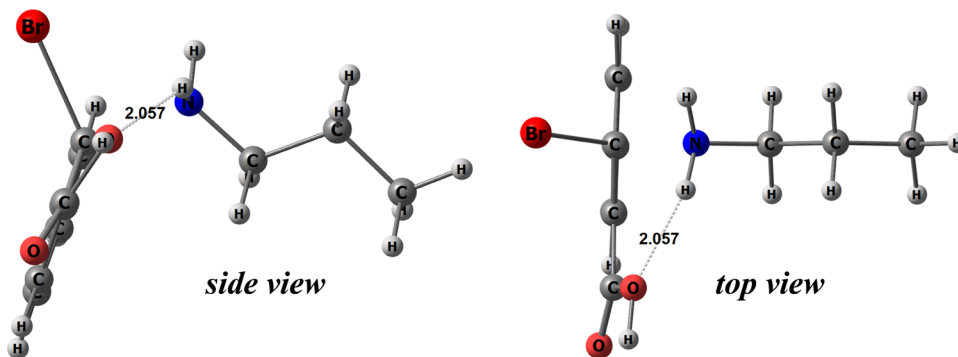
corrections (E_a^{ZPE}), which were computed as the energy differences between the confirmed TS structures and the relevant n-RPhX + NH$_2$R′ pairs [$E_a = E_{TS} − (E_{aryl} + E_{amine})$]. Table 1 also lists the corresponding activation free energy ($\Delta G_a^{298.15\,K}$). Since the IRC paths do not necessarily terminate to fully optimized geometries, the barrier heights listed in Table 1 were calculated as the difference in energy of the optimized TSSs and the isolated n-RPhX + NH$_2$R′ molecules. Additional data for these systems are given in Tables S1−S3 of the Supporting Information.

The values presented in Table 1 allow us to comment broadly on the effects of the R substituents on the halide elimination as well as the overall reaction. In general, barrier heights decrease as X gets larger and less electronegative. That is, the reaction becomes increasingly favorable as we go from X = Cl to I, reaffirming iodine as the best leaving group of the three halides considered—a well-known consequence of its low electronegativity, weaker C−X bond, and a significant relaxation in steric repulsion, as the iodine atom leaves.[45] For the very few cases in Table 1 where the ΔG value for X = Br is actually lower than it is for X = I (*i.e.*, 4-F and 4-CF$_3$), the margins are quite small (1.0 and 0.9 kJ mol^{-1}, respectively).

Overall, our work suggests that electron-withdrawing R groups are favorable for aryl amination, especially at the *ortho*-position. The lowest values were obtained for the 2-COOHPhX cases (for X = Br, and I), with ΔG values less than 164 kJ mol^{-1}. Electron-donating groups are found to be noticeably less favorable for the reaction, particularly when situated at the *para*-position. The highest ΔE_a^{ZPE} and $\Delta G_a^{298.15\,K}$ values have been calculated for the 4-MeOPhCl, 4-FPhCl, 4-MePhCl, and 2-MePhCl aminations with the NH$_2$^{n}Pr in Table 1. This agrees with the experimental work reported in Aubin et al.,[46] in which the presence of electron-withdrawing groups was found to be necessary to activate the halogen atom of aryl halides toward direct catalytic amination reactions with ammonia.

Within the subset of electron-withdrawing groups (*e.g.*, R = −CN and −CF$_3$) seen in Table 1, the *ortho*-substituted aryl rings are predicted to have, in general, the lowest barriers to reaction, whereas the *meta*-substituted cases are predicted to have the highest barriers. For the electron-donating substituents (*e.g.*, R = −Me and −OMe), *meta*-substitution yields the lowest barriers to amination—even if the *meta*- and *ortho*-barriers are only separated by <3 kJ mol^{-1}—whereas the *para*-substituted aryl halides yield the highest activation energies.
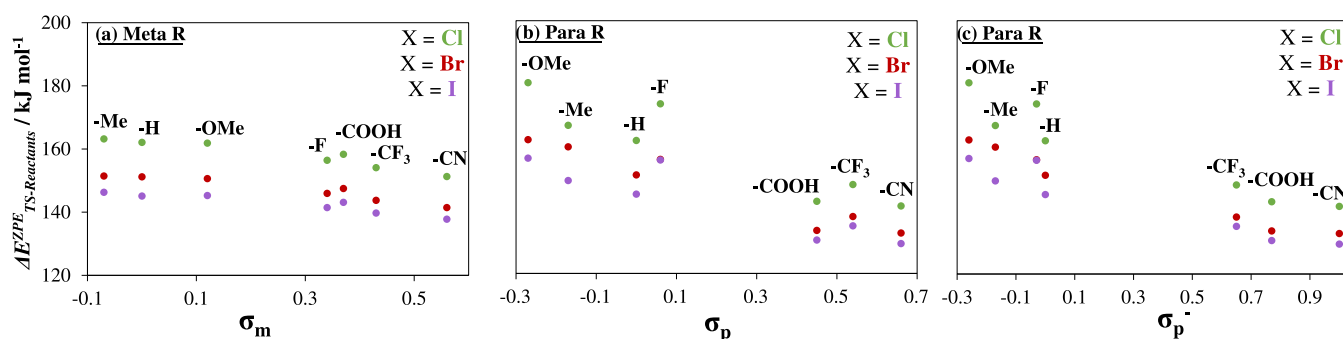

Figure 3. Side and top views of the transition state structure that links the 2-COOHPhBr + NH$_2$^{n}Pr′ reactants and the 2−COOHPhNH^{n}Pr′ + HBr products. The case shown here is qualitatively identical across all of the ortho R = −COOH compounds investigated in this work.

Figure 4. Zero-point energy-corrected barrier heights ($\Delta E_{\text{TS-Reactants}}^{\text{ZPE}}$) as functions of (a) σ_m, (b) σ_p, and (c) σ_p^- for the noncatalyzed n-RPhX + NH$_2$^{n}Pr amination, where R = −H, −Me, −OMe, −F, −CF$_3$, and −COOH; X = −Cl, −Br, and −I. All three graphs shown in Figure 4 share a common y-axis to illustrate the relative distribution of values for the *meta*- vs *para*-substituted cases.

The exceptionally low barriers predicted for the amination of the 2-COOHPhX molecule can be attributed to the size of the carboxyl group and a related proximity effect at the *ortho*-position that facilitates a stabilizing interaction with the amine during the reaction. We found strong geometrical evidence of an incipient hydrogen bond formation between one of the H atoms of the incoming amine and the saturated O of the −COOH group in 2-COOHPhX of the TSS shown in Figure 3. The IRC path data reveals that as the C−X bond rotates out of the plane away from the incoming amine, the COOH fragment rotates (though, to a lesser extent) toward the amine, thus establishing the hydrogen bonding interaction (Figure 3). This stabilizing hydrogen bond interaction appears to promote amination by lowering the activation energy for 2-COOHPhX relative to the n = 3 and 4 cases. Furthermore, the 2−COOHPhX molecule was found to have the lowest energy barrier despite the hydrogen bonding interaction appearing to result in a longer than typical C···N contact for its respective TSS (see Figure 2-left).

The modeling thus far has afforded us insights into the energetics of substituents systematically located around an aryl halide ring as well as a possible hydrogen bonding phenomena; however, this reaction, when implemented experimentally, likely proceeds through a benzyne intermediate pathway to allow for regioselective reactions.[4,18,20,45,47] A benzyne intermediate was not considered computationally herein, and therefore, regioselectivity was not accounted for in this work. A separate investigation for benzyne intermediates may be in order; however, such an analysis would require a sequence of calculations performed in stages to lead the reactions from reactants to products.[48,49]

Barrier Heights and Hammett Constants. To elucidate the relationship between the electronic influence from the substituents and the activation energies of the amination reactions, we employed the well-defined Hammett σ constants as quantitative approximations of the inductive effects of the substituents.[50] The Hammett σ constant is defined as $\sigma = (1/p)\cdot\log K/K_0$, where p is a dimensionless constant and K/K_0 is the ratio between the equilibrium constants of a given substituent (R) and an unsubstituted aromatic ring (R = −H). Based on the ratio of K to K_0, the σ values become more positive as substituents generally become more electron-withdrawing and more negative for more electron-donating substituents. Figure 4 shows the computed barrier heights ($\Delta E_{\text{TS-Reactants}}^{\text{ZPE}}$) as a function of the *meta*- and *para*-Hammett σ constants (σ_m and σ_p). A modified *para*-parameter, σ_p^-, which is defined using the ionization constants of *para*-substituted

phenols,[51] (ArOH $\rightleftarrows$ ArO$^-$ + H$^+$; $\sigma_p^- = 1/2.11 \log K/K_0$), is also shown in Figure 4.

For all three plots shown in Figure 4, the data points automatically fall into two categories based upon the particular σ values for each substituent, with the electron-donating and electron-withdrawing substituents appearing at the more negative and positive σ sides of the graphs, respectively. Excluding the anomalous case where R = −F, the energy barriers to amination generally decrease as the Hammett σ constants increase (going from *left* to *right* across Figure 4a−c); a pattern that is observed for both the *meta*- and *para*-substituted aryl halides (Figure 4a−c, respectively). It is also clear from Figure 4 that the activation energies for the *meta*-substituted systems fall within a somewhat narrower energy window compared to the *para*-substituted cases—an echo of the pattern mentioned previously for the C···X bond distances in the 3−R TSSs (see Figure 2d−f). The reaction barriers are generally *lower* for the *meta*-substituted cases compared to the *para*-substituted cases when the R groups are more electron-donating (comparing the data on the *left* sides of Figure 4a−c), but they are *higher* for the *meta*-substituted cases compared to the *para*-cases when R is more electron-withdrawing (comparing the data on the *right* sides of Figure 4a−c). This general pattern is seen for both σ_p and σ_p^-, since the two parameters broadly agree on the influence of the substituents.

For R = −F, the σ values seem to switch between the electron-poor and electron-rich subgroups of the substituents as we transition from *meta*- (Figure 4a) to *para*-substitutions (Figure 4b,c). This behavior is a consequence of the Hammett σ constants, reflecting the unique and well-studied differences in the impact of the inductive and mesomeric effects of the F atom on the benzene ring at *meta*- and *para*-positions. As an *ortho*-/*para*-director for electrophiles, R = −F appears to lower the barrier for a nucleophilic attack at the *meta*-position; however, as we pointed out above, the barriers for the *ortho*-case are not much higher. Furthermore, R = −F in the *para*-position has one of the most unfavorable amination energetics of the cases studied.

In brief, having electron-donating R groups as the *para*-substituent is found to be the least favorable arrangement position for the systems considered. The *ortho*-energies in Table 1 are consistently lower than the corresponding *para*-values. Again, the aryl halide amination reactions that we have considered are found to be the most favorable (having the lowest barriers) at the *meta*-position when the R group is electron-donating, whereas having R at the *ortho*-position is favorable when R is more electron-withdrawing. The influence

of the chain length of the alkyl amine (R′) for R′ = −Me, −Et, −nPr, and −nBu was also probed, and we observed no significant impact on the progress of the reaction in the gas phase (Table 2; additional details are presented in the Supporting Information, Tables S6 and S13).

Table 2. Activation and Reaction Free Energies (ΔG_a^T and ΔG_{rxn}^T) for the Noncatalyzed 4-MePhX + NH$_2^n$Pr Amination, Where X = −Cl and −Br

temp. (T) (°C)	ΔG_a^T (kJ mol^{-1})	ΔG_{rxn}^T (kJ mol^{-1})
	X = Cl	
−20	208.2	−16.4
25	216.2	−15.1
80	224.8	−13.4
	X = Br	
−20	197.4	−15.5
25	209.8	−14.9
80	214.3	−12.5

Temperature and Solvent Effects. To better approximate the experimental conditions for the amination of aryl halides, the 4-MePhX + NH$_2^n$Pr reaction was selected as our model system to investigate at various temperatures. For reactions considered thus far, the systems were optimized in the gas phase, and the free energies were obtained at 298.15 K (25 °C). The free energy data reported in Table 3 is for the 4-MePhX + NH$_2^n$Pr reaction at three temperatures (−20, 25, and 80 °C).

The activation free energies are found to be within 18 kJ mol^{-1} of each other across the temperature range considered for both X = −Cl and −Br, with an increase in the size of the barrier being observed as temperature increases. Thus, the change in the barrier height is expected to be relatively small across the span of a hundred degrees, on the assumption that temperature increases continuously across this range. Regardless of the magnitude, a general increase in the barrier height is predicted as the temperature increases.

The amination processes are slightly exergonic, with the computed $\Delta G_{rxn} < -17$ kJ mol^{-1} for both the X = −Cl and −Br cases shown in Table 3. So, the reactions are spontaneous,

Table 3. Barrier Heights (E_a^{ZPE} and ΔG_a^T) for the PhBr + NH$_2^n$Pr Amination at 80 °C for Various Solvent Conditions

ε_r	solvent	E_a^{ZPE} (kJ mol^{-1})	$\Delta G_a^{353.15\,K}$ (kJ mol^{-1})
1.00	vacuo	151.19	235.70
2.37	toluene	143.31	200.27
24.85	ethanol	135.34	191.71
35.00		135.03	191.36
37.22	DMF	134.98	191.31
50.00		134.79	191.10
65.00		134.66	190.95
78.36	water	134.58	190.87

but $|\Delta G_{rxn}|$ changes only by a few kJ mol^{-1} when the temperature changes by several degrees. The results that we have found for the 4-MePhX amination suggest, therefore, that the model reactions will be most favorable at lower temperatures with a decrease in the activation energy and an increasing stabilization of the products relative to the aryl halide and amine reactants.

An overview of the influence of solvents on the given amination reaction is presented by considering the specified dielectric constant values of common solvents. To minimize potentially substantial and unique influences of specific substituents on the solvent studies, we limit ourselves to an unsubstituted case, where R = −H. Solvent effects were examined for the PhBr + NH$_2^n$Pr amination at 80 °C—a reaction temperature in line with common experimental conditions for aminations in literature.[46,52] The dielectric constants of ε_r = 2.37, 24.85, 37.22, and 78.36 were employed via a PCM model, which correspond to toluene, ethanol, dimethylformamide (DMF), and water, respectively, as solvents. To sample across the range of permittivities more extensively, we included ε_r = 35.00, 50.00, and 65.00. Our results for the computed zero-point corrected energies and free energies are summarized in Table 3.

These results indicate that the activation energies will tend to decrease noticeably in solution compared to the gas phase. For example, a reduction in ΔG_a of about 35 kJ mol^{-1} is observed going from the gas phase to a reaction in toluene. The barrier height is lowest for water (E_a^{ZPE} = 138.4 kJ mol^{-1}), which has the highest relative permittivity that we considered, whereas the highest barrier height was for toluene (apart from the reaction in vacuo).

These results invite experimental investigations into the solvent dependence of aryl amination reactions. A 2003 report on the metal-free microwave-assisted aminations of electron-rich aryl halides found that the amination of bromobenzene with morpholine gave good yields (between 61 and 97% yields for 19 additional cases) for solvents with relatively high ε_r values with KO^{t}Bu, including DMF (ε_r = 36.7) and DMSO (ε_r = 46.7).[4] This effect may be attributed in part to the base, where NaOH and K$_2$CO$_3$ in DMSO gave yields of <1%. The reaction was similarly unsuccessful in toluene, benzene, and tetrachloromethane (all with ε_r < 3.0).[4] A low yield was also reported for CH$_3$CN, which has a dielectric constant comparable to that of DMF. Therefore, understanding the nature of the exact chemical environment can be decisive.

The computational observations of this work provide a template as well as a starting point for many possible investigations, including the incorporation of green solvents and approaches; modeling more complex substituents and reactants to resemble active pharmaceutical ingredient targets; modeling secondary and other amines to further aid in understanding the amination reaction; modeling and predicting regioselectivity and additional reaction mechanisms; modeling the roles and dynamics of bases computationally to account for experimental results; and gaining further understanding of how solvents with higher ε_r can lead to more favorable energetics of aryl aminations.

■ SUMMARY AND OUTLOOK

Aromatic C−N bond formation reactions remain an important area of development in organic chemistry. We contribute to that discussion in this work with an investigation into theoretical and fundamental aspects of the energetics of the amination process. The dependence of activation energy barriers on the nature and position of substituents on aryl halides was investigated while also considering the effects of varying the amine nucleophile alkyl chain lengths, reaction temperature, and solvent system. We find that categorization of the substituted aryl halides according to the relevant Hammett σ constants achieves a clear and instructive alignment between

the activation energies and the *ortho/para*-directing tendencies of a range of substituents on the aromatic ring. Evidence for a slow increase in the barriers to reaction and the exergonicity of the aryl amination reaction with temperature is reported. Furthermore, the dielectric constant of the solvent was found to have a substantial impact on the activation free energies and, by implication, on the success of the reaction. The computed activation energies decreased monotonously as the dielectric constants increased, with a significant reduction at a lower dielectric constant and a more gradual decrease thereafter. These observations provide insights for further explorations of aminations, especially with advancing efforts toward metal-free aryl aminations, nucleophilic substitutions, and greener solvents. A goal of this initial fundamental investigation of noncatalyzed processes has been to offer basic mechanistic and energetic insights into the metal-free process as the foundation for new experimental investigations as well.

COMPUTATIONAL METHODS

The optimized structural coordinates, harmonic vibrational frequency, and internal reaction coordinate (IRC) data reported in this work have been obtained using the B3LYP method using the Gaussian 09 suite of programs (G09).[53−55] For each case, the correlation-consistent triple-ζ (cc-pVTZ) basis sets were employed for all elements preceding iodine.[56] A small core (28-electron) multi-electron Dirac−Fock (MDF) relativistic effective core potential (without the spin-orbit part) and the corresponding cc-pVTZ basis set for valence electrons were employed for iodine.[57] The B3LYP functional was chosen as it has proven reliable for predicting qualitative trends in particular cases such as in barrier height calculations as well as reproducing experimental results.[58−62] The geometric and energetic data obtained at the B3LYP functional were compared to values computed with the B3LYP-D3 and ωB97XD methods (Supporting Information, Figure S1 and Tables S1, S4, and S5).[63−65] The robustness of the B3LYP data is evident in their quantitative agreement with the latter methods.

The Synchronous Transit-Guided Quasi-Newton (STQN) method was employed to examine the potential energy surfaces (PES) for reactions using the QST2 and QST3 options in G09, where an initial guess of the transition state was required for QST3. Viable transition state structures (TSSs) obtained in this way, which link the n-RPhX + NH_2R' reactants and the n-RPhNHR' + HX products (where n refers to the position of the substituent relative to X), were then reoptimized and confirmed to be first-order saddle points via harmonic vibrational frequency analyses. A refined picture of each reaction was achieved by calculating separately specific IRC pathways for each reaction using the confirmed TSSs. In that way, it was possible to generate in two dimensions a cross section of the potential energy surface (PES) that links the reactants, through the TS, to the products.[66,67]

Additionally, the activation energies corrected for zero-point energies and free energies, ΔE_a^{ZPE} and $\Delta G_a^{298.15\,K}$, have been computed for each reaction by summing the relevant energy values obtained from structural optimizations of the isolated reactant species and subtracting that sum from the corresponding TS structure energy values. Similarly, the free energies of the reactions were derived as the difference between the sum of the products and the sum of the reactant energies. For structures that have different conformations, we

made efforts to find the lowest energy conformer by comparing the relative energies of these structures.

Solvation effects have been studied with the implicit solvation model based on the self-consistent reaction field (SCRF) theory. For all product and reactant species examined in solution, geometry optimizations and frequency analyses were carried out using the polarizable continuum model (PCM).[68−71] All molecular representations were generated using the ChemDraw and Chemcraft programs.[72]

ASSOCIATED CONTENT

Ⓢ Supporting Information

The Supporting Information is available free of charge at https://pubs.acs.org/doi/10.1021/acsomega.1c03934.

Coordinates of minima and transition states, the zero-point corrected energies and free energies for reactions at different levels of theory (PDF)

AUTHOR INFORMATION

Corresponding Authors

Kelling J. Donald − *Department of Chemistry, University of Richmond, Richmond, Virginia 23173, United States;* ⓞ orcid.org/0000-0001-9032-4225; Email: kdonald@richmond.edu

B. Frank Gupton − *Department of Chemical and Life Science Engineering, Virginia Commonwealth University, Richmond, Virginia 23284, United States;* ⓞ orcid.org/0000-0002-8165-1088; Email: bfgupton@vcu.edu

Authors

Supreeth Prasad − *Department of Chemistry, University of California—Davis, Davis, California 95616, United States;* ⓞ orcid.org/0000-0003-3496-4388

Dylan D. Rodene − *Department of Chemical and Life Science Engineering, Virginia Commonwealth University, Richmond, Virginia 23284, United States;* ⓞ orcid.org/0000-0002-5235-4260

Michael B. Burkholder − *Department of Chemical and Life Science Engineering, Virginia Commonwealth University, Richmond, Virginia 23284, United States;* ⓞ orcid.org/0000-0003-1506-0260

Complete contact information is available at:
https://pubs.acs.org/10.1021/acsomega.1c03934

Notes

The authors declare no competing financial interest.

REFERENCES

(1) Brown, D. G.; Boström, J. Analysis of Past and Present Synthetic Methodologies on Medicinal Chemistry: Where Have All the New Reactions Gone? *J. Med. Chem.* **2016**, *59*, 4443−4458.

(2) Weissermel, K.; Arpe, H.-J. *Industrial Organic Chemistry*, 3rd ed.; Sora, K., Ed.; VCH Publishers, Inc.: New York, NY, 1997.

(3) Lawrence, S. A. *Amines: Synthesis, Properties and Applications*; Cambridge University Press, 2004; Vol. 1.

(4) Shi, L.; Wang, M.; Fan, C. A.; Zhang, F. M.; Tu, Y. Q. Rapid and Efficient Microwave-Assisted Amination of Electron-Rich Aryl

Halides without a Transition-Metal Catalyst. *Org. Lett.* **2003**, *5*, 3515−3517.

(5) Voth, S.; Hollett, J. W.; Mccubbin, J. A. Transition-Metal-Free Access to Primary Anilines from Boronic Acids and a Common +NH2 Equivalent. *J. Org. Chem.* **2015**, *80*, 2545−2553.

(6) Pant, P. L.; Shankarling, G. S. Recent Advances in Synthetic Methodologies for Transition Metal-Free Ullmann Condensation. *New J. Chem.* **2018**, *42*, 13212−13224.

(7) Seifinoforest, B.; Tanbakouchian, A.; Larijani, B.; et al. Ullmann-Goldberg and Buchwald-Hartwig C-N Cross Couplings: Synthetic Methods to Pharmaceutically Potential N-Heterocycles. *Asian J. Org. Chem.* **2021**, *10*, 1319−1344.

(8) Kosugi, M.; Kameyama, M.; Migita, T. Palladium-Catalyzed Aromatic Amination of Aryl Bromides with N,N-Di-Ethylamino-Tributyltin. *Chem. Lett.* **1983**, *12*, 927−928.

(9) Paul, F.; Patt, J.; Hartwig, J. F. Palladium-Catalyzed Formation of Carbon-Nitrogen Bonds. Reaction Intermediates and Catalyst Improvements in the Hetero Cross-Coupling of Aryl Halides and Tin Amides. *J. Am. Chem. Soc.* **1994**, *116*, 5969−5970.

(10) Guram, A. S.; Buchwald, S. L. Palladium-Catalyzed Aromatic Animations with in Situ Generated Aminostannanes. *J. Am. Chem. Soc.* **1994**, *116*, 7901−7902.

(11) Louie, J.; Hartwig, J. F. Palladium-Catalyzed Synthesis of Arylamines from Aryl Halides. Mechanistic Studies Lead to Coupling in the Absence of Tin Reagents. *Tetrahedron Lett.* **1995**, *36*, 3609−3612.

(12) Guram, A. S.; Rennels, R. A.; Buchwald, S. L. A Simple Catalytic Method for the Conversion of Aryl Bromides to Arylamines. *Angew. Chem. Int. Ed. Engl.* **1995**, *34*, 1348−1350.

(13) Wolfe, J. P.; Wagaw, S.; Buchwald, S. L. An Improved Catalyst System for Aromatic Carbon-Nitrogen Bond Formation: The Possible Involvement of Bis(Phosphine) Palladium Complexes as Key Intermediates. *J. Am. Chem. Soc.* **1996**, *118*, 7215−7216.

(14) Driver, M. S.; Hartwig, J. F. A Second-Generation Catalyst for Aryl Halide Amination: Mixed Secondary Amines from Aryl Halides and Primary Amines Catalyzed by (DPPF)PdCl2. *J. Am. Chem. Soc.* **1996**, *118*, 7217−7218.

(15) Marion, N.; Navarro, O.; Mei, J.; Stevens, E. D.; Scott, N. M.; Nolan, S. P. Modified (NHC)Pd(Allyl)Cl (NHC = N-Heterocyclic Carbene) Complexes for Room-Temperature Suzuki-Miyaura and Buchwald-Hartwig Reactions. *J. Am. Chem. Soc.* **2006**, *128*, 4101−4111.

(16) Guari, Y.; Es, D. S. van.; Reek, J. N. H.; Kamer, P. C. J.; Leeuwen, P. W. N. M. van. An Efficient, Palladium-Catalysed, Amination of Aryl Bromides. *Tetrahedron Lett.* **1999**, *40*, 3789−3790.

(17) Johnson, C. R.; Ansari, M. I.; Coop, A. Tetrabutylammonium Bromide-Promoted Metal-Free, Efficient, Rapid, and Scalable Synthesis of N-Aryl Amines. *ACS Omega* **2018**, *3*, 10886−10890.

(18) Chen, J.; Wu, J. Transition-Metal-Free C3 Arylation of Indoles with Aryl Halides. *Angew. Chem., Int. Ed.* **2017**, *56*, 3951−3955.

(19) Radhika, S.; Neetha, M.; Aneeja, T.; Anilkumar, G. Microwave-Assisted Amination Reactions: An Overview. *Curr. Org. Chem.* **2020**, *24*, 2235−2255.

(20) Sun, C.; Shi, Z. Transition-Metal-Free Coupling Reactions. *Chem. Rev.* **2014**, *114*, 9219−9280.

(21) Xu, G.; Wang, Y. Microwave-Assisted Amination from Aryl Triflates without Base and Catalyst. *Org. Lett.* **2004**, *6*, 985−987.

(22) Samadi, A.; Silva, D.; Chioua, M.; Carreiras, M. doC.; Marco-Contelles, J. Microwave Irradiation-Assisted Amination of 2-Chloropyridine Derivatives with Amide Solvents. *Synth. Commun.* **2011**, *41*, 2859−2869.

(23) Perin, N.; Hranjec, M.; Pavlović, G.; Karminski-Zamola, G. Novel Aminated Benzimidazo[1,2-a]Quinolines as Potential Fluorescent Probes for DNA Detection: Microwave-Assisted Synthesis, Spectroscopic Characterization and Crystal Structure Determination. *Dyes Pigments* **2011**, *91*, 79−88.

(24) Saulnier, M. G.; Zimmermann, K.; Struzynski, C. P.; Sang, X.; Velaparthi, U.; Wittman, M.; Frennesson, D. B. Microwave-Assisted Synthesis of Primary Amine HX Salts from Halides and 7 M Ammonia in Methanol. *Tetrahedron Lett.* **2004**, *45*, 397−399.

(25) Baqi, Y.; Muller, C. E. Catalyst-Free Microwave-Assisted Amination of 2-Chloro-5-Nitrobenzoic Acid. *J. Org. Chem.* **2007**, *72*, 5908−5911.

(26) Quevedo, C. E.; Bavetsias, V.; Mcdonald, E. Microwave-Assisted Synthesis of 2-Aminonicotinic Acids by Reacting 2-Chloronicotinic Acid with Amines. *Tetrahedron Lett.* **2009**, *50*, 2481−2483.

(27) Perin, N.; Bobanović, K.; Zlatar, I.; Jelić, D.; Kelava, V.; Koštrun, S.; Marković, V. G.; Brajša, K.; Hranjec, M. Antiproliferative Activity of Amino Substituted Benzo[b]Thieno[2,3-b]Pyrido[1,2-a]Benzimidazoles Explored by 2D and 3D Cell Culture System. *Eur. J. Med. Chem.* **2017**, *125*, 722−735.

(28) Chen, X.; Cui, X.; Yang, F.; Wu, Y. Base-Promoted Cross-Dehydrogenative Coupling of Quinoline N - Oxides with 1,3-Azoles. *Org. Lett.* **2015**, *17*, 1445−1448.

(29) Li, Y. W.; Zheng, H. X.; Yang, B.; Shan, X. H.; Qu, J. P.; Kang, Y. B. tBuOK-Promoted Cyclization of Imines with Aryl Halides. *Org. Lett.* **2020**, *22*, 4553−4556.

(30) Yang, C.; Zhang, F.; Deng, G.; Gong, H. Amination of Aromatic Halides and Exploration of the Reactivity Sequence of Aromatic Halides. *J. Org. Chem.* **2019**, *84*, 181−190.

(31) Hamann, B. C.; Hartwig, J. F. Systematic Variation of Bidentate Ligands Used in Aryl Halide Amination. Unexpected Effects of Steric, Electronic, and Geometric Perturbations. *J. Am. Chem. Soc.* **1998**, *120*, 3694−3703.

(32) Hartwig, J. F.; Richards, S.; Barañano, D.; Paul, F. Influences on the Relative Rates for C-N Bond-Forming Reductive Elimination and β-Hydrogen Elimination of Amides. A Case Study on the Origins of Competing Reduction in the Palladium-Catalyzed Amination of Aryl Halides. *J. Am. Chem. Soc.* **1996**, *118*, 3626−3633.

(33) Shekhar, S.; Hartwig, J. F. Effects of Bases and Halides on the Amination of Chloroarenes Catalyzed by Pd(P^{t}Bu$_3$)$_2$. *Organometallics* **2007**, *26*, 340−351.

(34) Hoi, K. H.; Çalimsiz, S.; Froese, R. D. J.; Hopkinson, A. C.; Organ, M. G. Amination with Pd-NHC Complexes: Rate and Computational Studies on the Effects of the Oxidative Addition Partner. *Chem. - A Eur. J* **2011**, *17*, 3086−3090.

(35) Hoi, K. H.; Çalimsiz, S.; Froese, R. D. J.; Hopkinson, A. C.; Organ, M. G. Amination with Pd-NHC Complexes: Rate and Computational Studies Involving Substituted Aniline Substrates. *Chem. - A Eur. J* **2012**, *18*, 145−151.

(36) McMullin, C. L.; Rühle, B.; Besora, M.; Orpen, A. G.; Harvey, J. N.; Fey, N. Computational Study of P^{t}Bu$_3$ as Ligand in the Palladium-Catalysed Amination of Phenylbromide with Morpholine. *J. Mol. Catal. A Chem.* **2010**, *324*, 48−55.

(37) Barder, T. E.; Biscoe, M. R.; Buchwald, S. L. Structural Insights into Active Catalyst Structures and Oxidative Addition to (Biaryl)-Phosphine - Palladium Complexes via Density Functional Theory and Experimental Studies. *Organometallics* **2007**, *26*, 2183−2192.

(38) Barder, T. E.; Buchwald, S. L. Insights into Amine Binding to Biaryl Phosphine Palladium Oxidative Addition Complexes and Reductive Elimination from Biaryl Phosphine Arylpalladium Amido Complexes via Density Functional Theory. *J. Am. Chem. Soc.* **2007**, *129*, 12003−12010.

(39) Cundari, T. R.; Deng, J. Density Functional Theory Study of Palladium-Catalyzed Aryl-Nitrogen and Aryl-Oxygen Bond Formation. *J. Phys. Org. Chem.* **2005**, *18*, 417−425.

(40) Green, J. C.; Herbert, B. J.; Lonsdale, R. Oxidative Addition of Aryl Chlorides to Palladium N-Heterocyclic Carbene Complexes and Their Role in Catalytic Arylamination. *J. Organomet. Chem.* **2005**, *690*, 6054−6067.

(41) Hamlin, T. A.; Swart, M.; Bickelhaupt, F. M. Nucleophilic Substitution (SN$_2$): Dependence on Nucleophile, Leaving Group, Central Atom, Substituents, and Solvent. *ChemPhysChem* **2018**, *19*, 1315−1330.

(42) Senger, N. A.; Bo, B.; Cheng, Q.; Kee, J. R.; Gronert, S.; Wu, W. The Element Effect Revisited: Factors Determining Leaving

Group Ability in Activated Nucleophilic Aromatic Substitution Reactions. *J. Org. Chem.* **2012**, *77*, 9535−9540.

(43) Ertl, P. Cheminformatics Analysis of Organic Substituents: Identification of the Most Common Substituents, Calculation of Substituent Properties, and Automatic Identification of Drug-Like Bioisosteric Groups. *J. Chem. Inf. Comput. Sci.* **2003**, *43*, 374−380.

(44) Truhlar, D. G.; Garrett, B. C.; Klippenstein, S. J. Current Status of Transition-State Theory. *J. Phys. Chem. A* **1996**, *100*, 12771−12800.

(45) Guo, D.; Huang, H.; Xu, J.; Jiang, H.; Liu, H. Efficient Iron-Catalyzed N-Arylation of Aryl Halides with Amines. *Org. Lett.* **2008**, *10*, 4513−4516.

(46) Aubin, Y.; Fischmeister, C.; Thomas, C. M.; Renaud, J. L. Direct Amination of Aryl Halides with Ammonia. *Chem. Soc. Rev.* **2010**, *39*, 4130−4145.

(47) Fujita, M.; Kim, W. H.; Sakanishi, Y.; Fujiwara, K.; Hirayama, S.; Okuyama, T.; Ohki, Y.; Tatsumi, K.; et al. Elimination - Addition Mechanism for Nucleophilic Substitution Reaction of Cyclohexenyl Iodonium Salts and Regioselectivity of Nucleophilic Addition to the Cyclohexyne Intermediate. *J. Am. Chem. Soc.* **2004**, *126*, 7548−7558.

(48) Domingo, L. R.; Rhyman, L.; Ríos-guti, M. Unveiling the High Reactivity of Benzyne in the Formal [3+2] Cycloaddition Reactions towards Thioamides through the Molecular Electron Density Theory. *Tetrahedron* **2020**, *76*, 1−10.

(49) Evoniuk, C. J.; dos Passos Gomes, G.; Hill, S. P.; Fujita, S.; Hanson, K.; Alabugin, I. V. Coupling N-H Deprotonation, C-H Activation, and Oxidation: Metal-Free C(Sp3)-H Aminations with Unprotected Anilines. *J. Am. Chem. Soc.* **2017**, *139*, 16210−16221.

(50) Hammett, L. P. The Effect of Structure upon the Reactions of Organic Compounds. Benzene Derivatives. *J. Am. Chem. Soc.* **1937**, *59*, 96−103.

(51) Hansch, C.; Leo, A.; Taft, R. W. A Survey of Hammett Substituent Constants and Resonance and Field Parameters. *Chem. Rev.* **1991**, *91*, 165−195.

(52) Conesa Lerma, I.; Cawley, M. J.; Cloke, F. G. N.; Arentsen, K.; Scott, J. S.; Pearson, S. E.; Hayler, J.; Caddick, S. Studies on Pd/ Imidazolium Salt Protocols for Aminations of Aryl Bromides and Iodides Using Lithium Hexamethyldisilazide (LHMDS). *J. Organomet. Chem.* **2005**, *690*, 5841−5848.

(53) Becke, A. D. Density-Functional Thermochemistry. III. The Role of Exact Exchange. *J. Chem. Phys.* **1993**, *98*, 5648−5652.

(54) Stephens, P. J.; Devlin, F. J.; Chabalowski, C. F.; Frisch, M. J. Ab Initio Calculation of Vibrational Absorption and Circular Dichroism Spectra Using Density Functional Force Fields. *J. Phys. Chem. B.* **1994**, *98*, 11623−11627.

(55) Frisch, M. J.; Trucks, G. W.; Schlegel, H. B.; Scuseria, G. E.; Robb, M. A.; Cheeseman, J. R.; Scalmani, G.; Barone, V.; Mennucci, B.; Petersson, G. A.; Al, E.. *Gaussian 09.* Gaussian, Inc.: Wallingford, CT, 2013.

(56) Dunning, T. H. Gaussian Basis Sets for Use in Correlated Molecular Calculations. I. The Atoms Boron through Neon and Hydrogen. *J. Chem. Phys.* **1989**, *90*, 1007−1023.

(57) Peterson, K. A.; Shepler, B. C.; Figgen, D.; Stoll, H. On the Spectroscopic and Thermochemical Properties of ClO, BrO, IO, and Their Anions. *J. Phys. Chem. A* **2006**, *110*, 13877−13883.

(58) Ermanis, K.; Colgan, A. C.; Proctor, R. S. J.; Hadrys, B. W.; Phipps, R. J.; Goodman, J. M. A Computational and Experimental Investigation of the Origin of Selectivity in the Chiral Phosphoric Acid Catalyzed Enantioselective Minisci Reaction. *J. Am. Chem. Soc.* **2020**, *142*, 21091−21101.

(59) Chatterjee, N.; Arfeen, M.; Bharatam, P. V.; Goswami, A. A Metal and Base-Free Chemoselective Primary Amination of Boronic Acids Using Cyanamidyl/Arylcyanamidyl Radical as Aminating Species: Synthesis and Mechanistic Studies by Density Functional Theory. *J. Org. Chem.* **2016**, *81*, 5120−5127.

(60) Riley, K. E.; Op't Holt, B. T.; Merz, K. M. Critical Assessment of the Performance of Density Functional Methods for Several Atomic and Molecular Properties. *J. Chem. Theory Comput.* **2007**, *3*, 407−433.

(61) Ignatyev, I.; Montejo, M.; Ortega, P. G. R.; Gonzalez, J. J. L. Effect of Substituents and Hydrogen Bonding on Barrier Heights in Dehydration Reactions of Carbon and Silicon Geminal Diols. *Phys. Chem. Chem. Phys.* **2011**, *13*, 18507−18515.

(62) Tirado-Rives, J.; Jorgensen, W. L. Performance of B3LYP Density Functional Methods for a Large Set of Organic Molecules. *J. Chem. Theory Comput.* **2008**, *4*, 297−306.

(63) Grimme, S.; Antony, J.; Ehrlich, S.; Krieg, H. A Consistent and Accurate Ab Initio Parametrization of Density Functional Dispersion Correction (DFT-D) for the 94 Elements H-Pu. *J. Chem. Phys.* **2010**, *132*, No. 154104.

(64) Chai, J. Da.; Head-Gordon, M. Long-Range Corrected Hybrid Density Functionals with Damped Atom-Atom Dispersion Corrections. *Phys. Chem. Chem. Phys.* **2008**, *10*, 6615−6620.

(65) Chai, J.-D.; Head-Gordon, M. Systematic Optimization of Long-Range Corrected Hybrid Density Functionals. *J. Chem. Phys.* **2008**, *128*, No. 084106.

(66) Fukui, K. A. Formulation of the Reaction Coordinate. *J. Phys. Chem. C.* **1970**, *74*, 4161.

(67) Fukui, K. The Path of Chemical Reactions - The IRC Approach. *Acc. Chem. Res.* **1981**, *14*, 363−368.

(68) Cancès, E.; Mennucci, B.; Tomasi, J. A New Integral Equation Formalism for the Polarizable Continuum Model: Theoretical Background and Applications to Isotropic and Anisotropic Dielectrics. *J. Chem. Phys.* **1997**, *107*, 3032−3041.

(69) Tomasi, J.; Persico, M. Molecular Interactions in Solution: An Overview of Methods Based on Continuous Distributions of the Solvent. *Chem. Rev.* **1994**, *94*, 2027−2094.

(70) Tomasi, J.; Mennucci, B.; Cammi, R. Quantum Mechanical Continuum Solvation Models. *Chem. Rev.* **2005**, *105*, 2999−3093.

(71) Barone, V.; Cossi, M. Quantum Calculation of Molecular Energies and Energy Gradients in Solution by a Conductor Solvent Model. *J. Phys. Chem. A* **1998**, *102*, 1995−2001.

(72) *Chemcraft - Graphical Software for Visualization of Quantum Chemistry Computations*, http://www.chemcraftprog.com.